

DNS SLAM: Dense Neural Semantic-Informed SLAM

Kunyi Li¹ Michael Niemeyer² Nassir Navab^{1,3} Federico Tombari^{1,2}
¹Technical University of Munich ²Google ³Johns Hopkins University

Abstract

In recent years, coordinate-based neural implicit representations have shown promising results for the task of Simultaneous Localization and Mapping (SLAM). While achieving impressive performance on small synthetic scenes, these methods often suffer from oversmoothed reconstructions, especially for complex real-world scenes. In this work, we introduce DNS SLAM, a novel neural RGB-D semantic SLAM approach featuring a hybrid representation. Relying only on 2D semantic priors, we propose the first semantic neural SLAM method that trains class-wise scene representations while providing stable camera tracking at the same time. Our method integrates multi-view geometry constraints with image-based feature extraction to improve appearance details and to output color, density, and semantic class information, enabling many downstream applications. To further enable real-time tracking, we introduce a lightweight coarse scene representation which is trained in a self-supervised manner in latent space. Our experimental results achieve state-of-the-art performance on both synthetic data and real-world data tracking while maintaining a commendable operational speed on off-the-shelf hardware. Further, our method outputs class-wise decomposed reconstructions with better texture capturing appearance and geometric details.

1. Introduction

Dense Visual Simultaneous Localization and Mapping (SLAM) is a fundamental problem in the field of computer vision and plays a crucial role in various applications such as autonomous driving, indoor robotics, mixed reality, and more. Its primary goal is to create a 3D map of an unknown environment while simultaneously estimating camera poses. Traditional SLAM systems [7, 13, 16, 25] rely on multi-view geometry and focus more on camera pose accuracy but are prone to trajectory drifting. Recent learning-based dense visual SLAM methods [7, 11, 12, 14, 33, 38, 40, 42–44, 54] have aimed instead to generate meaningful global 3D maps, albeit with limited reconstruction accuracy and demanding extensive training for accurate pose estimation.

Inspired by the advancements in neural field research,

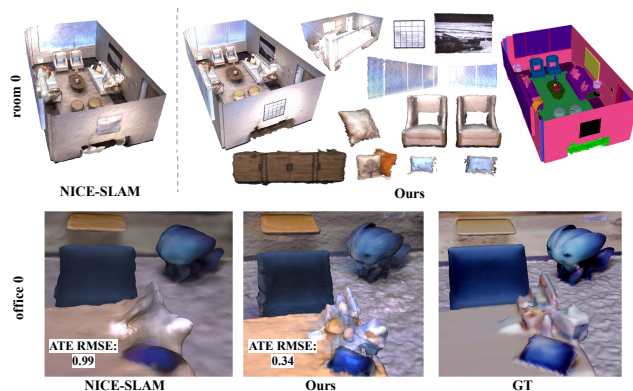


Figure 1. **Class-Wise Reconstruction using DNS SLAM.** In contrast to previous neural SLAM systems, our method leads to semantically-decomposed 3D reconstructions of the scene (top) required for many downstream applications. Further, by using image-based features, we improve camera tracking and our reconstructions contain more geometric and appearance details (bottom).

neural implicit SLAM methods like iMAP [38] and NICE-SLAM [54] have recently emerged. These methods estimate poses from a scene representation, prioritizing world-space geometry over image-space geometry, showing promising results on synthetic indoor datasets. They leverage the inherent smoothness and coherence encoded in Multilayer Perceptron (MLP) weights, making them suitable for sequential tracking and mapping tasks. However, these methods tend to oversmooth details in the reconstruction, which causes additional tracking errors. To address this challenge, Co-SLAM [42] uses parametric embeddings, while Point-SLAM [33] combines point cloud data with neural implicit representations to enhance reconstruction details. However, we find that their remarkable performance heavily relies on accurate pixel-perfect depth supervision. But in the real-world the depth is usually noisy, and we observe that these methods degenerate drastically in these scenarios.

For robotics and interactive real-world vision applications, a semantic model that represents scene classes separately is required. vMAP [17] excels at accurate and complete scene reconstruction by modeling objects separately, but focuses only on reconstruction and does not perform localization.

To bridge the gap and fully leverage multi-view geometry and semantic information, we introduce Dense Neural Semantic-Informed (DNS) SLAM. Our method utilizes class-wise scene representations which can build constraints between each class and the current camera pose. Further, 2D features from reference images provide multi-view geometry constraints for better camera pose estimation. In summary, our main **contributions** include:

- Leveraging 2D semantic priors, we investigate a semantic-informed multi-class scene representation, yielding an efficient, comprehensive, and semantically decomposed geometry representation.
- Utilizing multi-view geometry, we extract image features by back-projecting points into reference frames, establishing constraints on relative camera poses and enhancing the appearance details.
- To speed up tracking, we introduce a lightweight coarse scene representation which is trained with a novel self-supervision strategy, utilizing the multi-class representation as pseudo ground-truth.
- To achieve accurate and smooth reconstructions, we approximate occupancy probabilities with Gaussian distributions as the ground-truth for additional geometry supervision.

Compared with state-of-the-art (SOTA) methods, our method achieves better performance on camera pose estimation on both synthetic and real-world datasets, improving ATE RMSE over 10% on average.

2. Related Work

Scene Representations. Since the introduction of neural fields in the context of 3D reconstruction [4, 20, 30], they have been applied to many 3D computer vision tasks, including novel view synthesis [22], semantic scene reconstruction [51], and camera pose estimation [2]. Approaches such as Neural Radiance Fields (NeRF) [21] have achieved remarkable scene reconstruction results through differentiable rendering. However, it’s worth noting that coordinate-based encoding methods [1, 6, 8, 13, 43–45, 48, 54] come with the drawback of extended training times. To mitigate this, recent approaches [15, 24, 28] employ parametric encoding techniques expediting the training process. This enables neural implicit methods for real-time SLAM applications. While some works focus on improving the efficiency, Pixel-NeRF [47] preserves the spatial alignment between images and 3D representation, which is also an important concept in SLAM, by extracting 2D features from reference images and operating in view-space. Semantic-NeRF [51] provides precise geometry and semantic outcomes even with minimal semantic guidance. This demonstrates that with solely 2D semantic supervision, neural implicit methods can generate compelling 3D semantic scene reconstruction. For real-world SLAM applications, a semantic model is undoubtedly more

meaningful. Our work partly builds upon the foundations of both Pixel-NeRF and Semantic-NeRF, but takes a significant step forward by simultaneously optimizing the camera poses while they assuming pose data is given.

Dense Visual SLAM. Modern SLAM methods follow the overall architecture introduced by MonoSLAM [7], PTAM [16] and ORB SLAM [25], decomposing the task into mapping and tracking. Based on the working space of map reconstruction, SLAM methods can be generally divided into two categories: image view-centric space and world view-centric space. The former one aims at maintaining multi-view geometry among keyframes in the dense setting, and the later one anchors the 3D geometry representation in a uniform world coordinate. DTAM [26] is an early example of image view-centric methods and has been adapted in many recent learning-based SLAM system [3, 37, 39, 50]. DeepTAM [52] combines the cost volume and keyframe image to update the depth prediction. D3VO [46] models the photometric uncertainties of pixels on the input images, which improves the depth estimation accuracy. And Droid SLAM [40] uses optical flow to define geometrical residuals. World view-centric methods store global map in surfels [34, 45], octrees [41] or grids like voxel grid [6, 13, 43–45] and hash grid [15, 28]. KinectFusion [13] performs a frame-to-model camera tracking strategy and updates the scene geometry via Truncated Signed Distance Function (TSDF) fusion. RoutedFusion [43] outputs the TSDF update of the volumetric grid. NeuralFusion [44] extends this concept by learning the scene representation implicitly. In our method, the benefits from both image view and world are adopted, using a hybrid scene representation.

Neural Implicit SLAM. More recently, there has been a popularity in neural implicit representations for dense visual SLAM. iMAP [38], as the first neural implicit SLAM method, employs an MLP-based representation to conduct joint tracking and mapping in quasi-real time, but the reconstruction and camera pose result are far worse than traditional methods. To address computational overhead and scalability, NICE-SLAM [54] introduces a multi-level feature grid as scene representation. Nevertheless, the feature grid’s local update approach limits its hole-filling capabilities. On the other hand, Co-SLAM [42] attains real-time performance by combining coordinate and sparse parametric encodings for scene representation, employing dense global bundle adjustment using rays sampled from all keyframes. E-SLAM [14] suggests the use of multi-scale axis-aligned feature planes to prevent the model size from growing cubically concerning the scene’s size. Point-SLAM [33] introduces a neural point cloud that iteratively grows in a data-driven manner during scene exploration for both mapping and tracking. ADFP [11] proposes an attentive depth fusion prior and uses either currently learned geometry or the one from depth fusion in volume rendering.

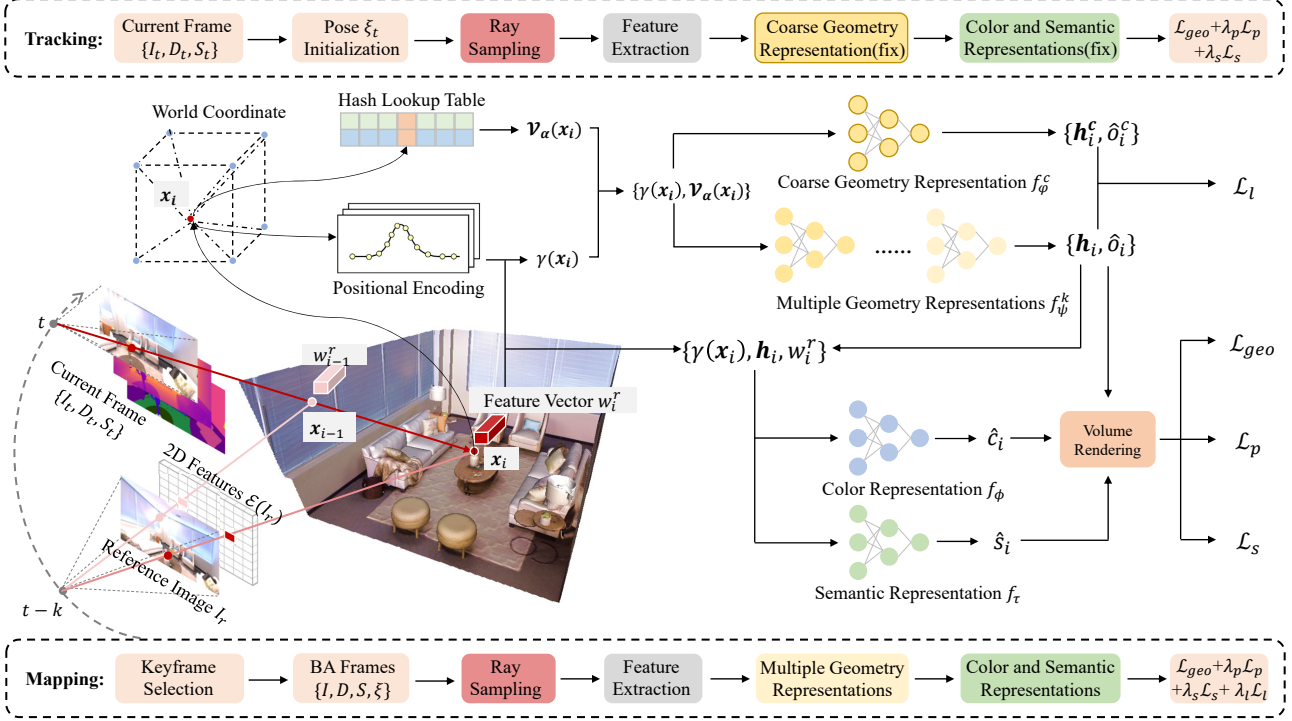


Figure 2. **Overview.** 1) Scene Representation: For each point along the ray, we first query a 3D feature from our hash-based feature grid and a 2D feature from reference image(s). Next, we use multiple geometry together with color and semantic representations to render occupancy, color, semantic logits to 2D. 2) Tracking: We optimize per-frame camera poses by utilizing a coarse geometry representation which in turn is trained in a self-supervised manner using our fine decomposed representation. 3) Mapping: In global and local bundle adjustment, we jointly optimize the scene representation and camera poses.

3. Method

3.1. Scene Representation

Notation: Let $\xi_t^{c2w} = [R_t^{c2w} | \mathbf{t}_t^{c2w}] \in SE(3)$ be the camera-to-world transform of frame t , where $R_t^{c2w} \in SO(3)$ and $\mathbf{t}_t^{c2w} \in \mathbb{R}^3$ are the rotation and translation, respectively. Denote camera intrinsic matrix as $K \in \mathbb{R}^{3 \times 3}$. For the rest of the manuscript we set $\xi = \xi^{c2w}$ to avoid cluttered notation. Camera projection and back-projection operator is denoted as π^{-1} and π , respectively, where π maps a 3D point \mathbf{x}^c in the camera coordinate system into the image coordinate system and π^{-1} maps a pixel \mathbf{u} in image coordinate system with depth $d(\mathbf{u})$ into the camera coordinate system:

$$\pi(\mathbf{x}^c) \cong K\mathbf{x}^c, \pi^{-1}(\mathbf{u}, d(\mathbf{u})) \cong d(\mathbf{u})K^{-1}\mathbf{u} \quad (1)$$

Note that we drop explicit homogeneous notation for clarity. **Neural Rendering:** The input of our SLAM system is a RGB-D and semantic label stream $\{I_t\}_{t=1}^T, \{D_t\}_{t=1}^T, \{S_t\}_{t=1}^T$ with known intrinsics K . Our goal is to estimate camera poses $\{\hat{\xi}_t\}_{t=1}^T$ and train a scene representation θ . Each pixel in image space $\mathbf{u} \in \mathbb{R}^2$ determines a ray in world space with origin $\mathbf{o} = \hat{\mathbf{t}}_t$ and ray direction $\mathbf{d} = \hat{R}_t K^{-1}\mathbf{u}$. For rendering, we randomly

sample M points $\mathbf{x}_i = \mathbf{o} + d_i \mathbf{d}, i \in \{1, \dots, M\}$ along the ray where d_i denotes depth value of sampled point \mathbf{x}_i . We use One-blob [23] encoding $\gamma(\mathbf{x}_i)$ similar to [42] and a multi-resolution hash-based feature grid $\mathcal{V}_\alpha = \{\mathcal{V}_\alpha^l\}_{l=1}^L$ [24] as geometry representation. Our method first maps \mathbf{x}_i into occupancy value \hat{o}_i and latent vector \mathbf{h}_i with geometry representation:

$$f_\psi(\gamma(\mathbf{x}_i), \mathcal{V}_\alpha(\mathbf{x}_i)) \mapsto (\mathbf{h}_i, \hat{o}_i). \quad (2)$$

We use multiple geometry representations f_ψ^k for each class in the scene instead of single one, which will be explained in Sec. 3.2. Then, the color representation predicts color value \hat{c}_i as:

$$f_\phi(\gamma(\mathbf{x}_i), \mathbf{h}_i) \mapsto \hat{c}_i. \quad (3)$$

Besides geometry and appearance, we further use a semantic representation to predict semantic logit value \hat{s}_i as:

$$f_\tau(\gamma(\mathbf{x}_i), \mathbf{h}_i) \mapsto \hat{s}_i. \quad (4)$$

We set all learnable parameters of our scene representation as $\theta = \{\alpha, \psi, \phi, \tau\}$. We render depth \hat{d} , color \hat{c} and semantic logit value \hat{s} by integrating the predicted values along the

sample rays [21, 29]:

$$\hat{\mathbf{g}} = \hat{\mathbf{g}}(\mathbf{u}; \hat{\xi}_t, \theta) = \sum_{i=1}^M w_i \hat{\mathbf{g}}_i, \quad (5)$$

where $\hat{\mathbf{g}} \in \{\hat{\mathbf{c}}, \hat{d}, \hat{\mathbf{s}}\}$. The weight w_i represents the discretized probability that the ray terminates at point \mathbf{x}_i :

$$w_i = \hat{o}_i \prod_{j=1}^{i-1} (1 - \hat{o}_j). \quad (6)$$

Like traditional SLAM methods [25], our method can be split into two processes: tracking and mapping. Tracking process first estimates camera pose of each frame while keeping the scene representations fixed. Mapping process jointly optimizes both the scene representations and camera poses. More details will be explained in the following sections. Fig. 2 shows an overview of our method.

3.2. Multi-Class Consistency

Instead of using a single shared MLP similar to previous neural SLAM approaches, decomposing the prediction into smaller class-specific MLPs can lead to a significant performance boost and speedup [17, 18, 31]. While obtaining 3D semantic priors is difficult in most cases, 2D semantic segmentation [19, 32, 53] is a well-studied task. As a result, in our method, we choose to utilize 2D semantic maps as they are often directly provided in datasets or alternatively can also be obtained from off-the-shelf methods. While we focus on class-level semantic maps in this work, other decompositions such as instance-level maps could be further explored in the future.

Multi-Class Rendering: For each pixel \mathbf{u} in the image, first the 2D semantic map is queried to obtain its corresponding class id $k = \mathbf{s}(\mathbf{u})$, where $\mathbf{s}(\mathbf{u})$ denotes ground-truth semantic label at pixel \mathbf{u} . In this case, scene representation Eq. 2 can be rewritten as:

$$f_{\psi}^k(\gamma(\mathbf{x}_i), \mathcal{V}_{\alpha}(\mathbf{x}_i)) \mapsto (\mathbf{h}_i, \hat{o}_i), \quad (7)$$

and density can be rendered as:

$$\hat{d} = \hat{d}(\mathbf{u}; \hat{\xi}, \psi^k) = \sum_{i=1}^M w_i \hat{o}_i, \quad (8)$$

where $k = 1, \dots, K$, denotes different class. Therefore, the geometry loss function can be expressed as:

$$\min \mathcal{L}_{geo} = \sum_{\mathbf{u} \in |I|} \left\| d(\mathbf{u}) - \hat{d}(\mathbf{u}; \hat{\xi}, \theta) \right\|_1 \quad (9)$$

where $d(\mathbf{u})$ denotes ground-truth depth value at pixel \mathbf{u} , and $|I|$ represents a set of pixels sampled from image I . We use the L_1 norm as our geometry loss \mathcal{L}_{geo} .

3.3. Multi-View Consistency

Previous neural implicit SLAM methods directly predict RGB colors from latent representations and they tend to lead to oversmoothed reconstructions. As shown in image-based rendering approaches such as Pixel-NeRF [47], spatial image features aligned to each pixel as an input allows the model to learn not only more texture information, but also scene priors. Therefore, we use features from 2D images as a conditional input in our model.

Image-Based Feature Pooling: Specifically, for every target frame I , we choose a reference frame I_r and extract 2D features $\mathcal{E}(I_r)$ using off-the-shelf method (ResNet-18 [10] in our case). Next, we cast rays for the target frame I to get sets of 3D points $\{\mathbf{x}_i\}$, and each 3D point $\mathbf{x}_i = \hat{\xi}_t \pi^{-1}(\mathbf{u}, d_i(\mathbf{u}))$ is back-projected to the reference frame coordinate to retrieve the corresponding image feature vectors \mathbf{w}_i^r :

$$\mathbf{w}_i^r = \mathcal{E}(I_r(\pi((\hat{\xi}_r)^{-1} \hat{\xi}_t \pi^{-1}(\mathbf{u}, d_i(\mathbf{u}))))). \quad (10)$$

Instead of directly passing these features to our scene representation, we encode each feature with the corresponding reference view $(\mathbf{o}_r, \mathbf{d}_r)$ to obtain intermediate feature vectors:

$$f_{\sigma}(\gamma(\mathbf{o}_r, \mathbf{d}_r), \mathbf{w}_i^r) \mapsto \bar{\mathbf{w}}_i^r, \quad (11)$$

where σ is the learnable parameters. In multi-reference frames case, feature vectors from each frame are then aggregated with an average pooling operator as the final image feature vector $\mathbf{w}_i = (\sum_{r=1}^N \bar{\mathbf{w}}_i^r) / N$. With image feature as conditional input, the color and semantic representation Eq. 3 and Eq. 4 can be rewritten as:

$$f_{\phi}(\gamma(\mathbf{x}_i), \mathbf{h}_i, \mathbf{w}_i) \mapsto \hat{\mathbf{c}}_i, \quad (12)$$

$$f_{\tau}(\gamma(\mathbf{x}_i), \mathbf{h}_i, \mathbf{w}_i) \mapsto \hat{\mathbf{s}}_i. \quad (13)$$

Color $\hat{\mathbf{c}}(\mathbf{u}; \hat{\xi}_t, \theta)$ and semantic logits $\hat{\mathbf{s}}(\mathbf{u}; \hat{\xi}_t, \theta)$ are rendered as in Eq. 5. The photometric and semantic loss are defined as:

$$\mathcal{L}_p = \sum_{\mathbf{u} \in |I|} \left\| \mathbf{c}(\mathbf{u}) - \hat{\mathbf{c}}(\mathbf{u}; \hat{\xi}_t, \theta) \right\|_2, \quad (14)$$

$$\mathcal{L}_s = - \sum_{\mathbf{u} \in |I|} \sum_{k=1}^K (\mathbf{s}^k(\mathbf{u}) \log(\hat{\mathbf{s}}^k(\mathbf{u}; \hat{\xi}_t, \theta))), \quad (15)$$

where $\mathbf{c}(\mathbf{u})$, $\mathbf{u}(\mathbf{x})$ are ground-truth color and semantic logits. For the photometric loss \mathcal{L}_p , we use the L_2 norm and for the semantic loss \mathcal{L}_s , we use multi-class cross-entropy loss.

3.4. Self-Supervised Coarse Scene Representation

SLAM requires real-time performance, but our multi-class scene representations can become hardware-intense on smaller-compute devices. To tackle this, we exploit the fact that while a single MLP is not ideal to represent an entire scene due to catastrophic forgetting, it can however be

used to represent a small neighborhood of the scene in a lightweight manner and is hence an ideal candidate for tracking. Thus, we introduce a lightweight coarse scene representation:

$$f_{\varphi}^c(\gamma(\mathbf{x}_i), \mathcal{V}_{\alpha}(\mathbf{x}_i)) \mapsto (\mathbf{h}_i^c, \hat{o}_i^c). \quad (16)$$

Instead of training this coarse scene representation separately, which is time consuming, latent multi-class scene representations are used to supervise it during mapping:

$$\mathcal{L}_l = \sum_{i=1} \|\mathbf{h}_i - \mathbf{h}_i^c\|_2, \quad (17)$$

where \mathbf{h}_i is latent vectors from Eq. 7. L_2 norm is applied on this self-supervised latent loss \mathcal{L}_l .

3.5. Occupancy Probability Approximation

To achieve accurate and smooth reconstructions with detailed geometry, we propose an occupancy probability approximation loss inspired by the approximate SDF and feature smoothness losses in [42]. Specifically, for samples within the truncation region, i.e., points where $|d_i - d(\mathbf{u})| \leq tr$, we assume the occupancy probability follows a Gaussian distribution with mean value at the observed distance:

$$o_i = f(|d_i - d(\mathbf{u})|; \mu, \sigma) = \frac{1}{\sigma\sqrt{2\pi}} e^{-\frac{1}{2}\left(\frac{|d_i - d(\mathbf{u}) - \mu|}{\sigma}\right)^2}. \quad (18)$$

We use this approximation as the ground-truth occupancy value for supervision:

$$\mathcal{L}_o = \sum_{\mathbf{u} \in |I|} \sum_{|d_i - d(\mathbf{u})| \leq tr} \|o_i - \hat{o}_i\|_2. \quad (19)$$

For points that are far from the surface $|d_i - d(\mathbf{u})| > tr$, we apply a free-space loss [27] which forces the occupancy to be zero:

$$\mathcal{L}_{fs} = \sum_{\mathbf{u} \in |I|} \sum_{|d_i - d(\mathbf{u})| > tr} \|\hat{o}_i\|_2. \quad (20)$$

3.6. Mapping

Our model consisting of a feature grid \mathcal{V}_{α} and scene representations $\theta = \{\alpha, \psi^k, \phi, \tau, \varphi\}$ are randomly initialized at the beginning. During the whole process, 2D feature encoder \mathcal{E} is fixed. For the first input frame, camera pose is fixed and only the hash grid and scene representations are optimized. For subsequent frames, scene representations and camera poses are optimized jointly and iteratively every k frames.

Keyframe Selection and BA: We follow [54] to choose the keyframes and frames for bundle adjustment (BA). For each mapping step, bundle adjustment is applied with current frame, the latest keyframe, and $W - 2$ selected keyframes. Instead of only carrying local BA, which means selecting $W - 2$ keyframes which has overlaps with current frame, we also randomly choose $W - 2$ keyframes from the whole keyframes for global BA.

Reference Frame Selection. We denote these selected BA frames as target frames. For each target frame, two reference frames are chosen by following strategy:

- for current frame, the two latest keyframes are chosen,
- for latest keyframe, two previous keyframes are chosen,
- for other keyframe, one previous keyframe and one later keyframe are chosen.

Ray Sampling: First, R pixels are randomly sampled from W target frames. 60% of them are randomly sampled among the image plane, 40% of them are randomly sampled among each class. Then, as described in Sec. 3.1, points are sampled along the rays. We use depth guided sampling such that M_s points are sampled near the surface and M_a points are sampled in free space.

New Class Initialization: If we encounter a previously unseen class, a new scene representation will be created and initialized. Then, it will be trained separately for 100 iterations before it joins the multi-class scene representations. This allows the system dynamically adding new class, which is more meaningful in practice.

Mapping Loss: Mapping process is performed via minimizing the loss functions with respect to the learnable parameters θ and camera poses ξ . The final loss \mathcal{L}_M is

$$\mathcal{L}_M(\theta, \xi) = \mathcal{L}_{geo} + \lambda_p \mathcal{L}_p + \lambda_s \mathcal{L}_s + \lambda_l \mathcal{L}_l + \lambda_o \mathcal{L}_o + \lambda_{fs} \mathcal{L}_{fs} \quad (21)$$

where $\lambda_p, \lambda_s, \lambda_l, \lambda_o, \lambda_{fs}$ are respective loss weighting factors.

3.7. Tracking

For tracking, the hash-based feature grid and the scene representations are fixed, and only the camera pose are updated. The latest optimized frame is chosen as the reference frame for extracting features and R_t pixels are randomly sampled among the whole image. We use the same ray sampling strategy as in mapping. Occupancy values \hat{o}_i^c and latent vectors \mathbf{h}_i^c are obtained by Eq. 16 and latent vectors are passed to Eq. 12 and Eq. 13 to obtain the color \hat{c}_i and semantic values \hat{s}_i .

Tracking Loss: A modified version of our geometry loss function is used in tracking, where the geometry term is weighted by the standard deviation of the depth prediction \hat{d}_{var} :

$$\mathcal{L}_{geo}^{track} = \sum_{\mathbf{u} \in |I|} \frac{\|d(\mathbf{u}) - \hat{d}(\mathbf{u}; \hat{\xi}_t, \theta)\|_1}{\sqrt{\hat{d}_{var}(\mathbf{u}; \hat{\xi}_t, \theta)}}, \quad (22)$$

where $\hat{d}_{var}(\mathbf{u}; \hat{\xi}_t, \theta) = \sum_{i=1}^M w_i (\hat{d}(\mathbf{u}; \hat{\xi}_t, \theta) - \hat{d}_i)^2$.

Given an initial guess of current camera pose and under the constant speed assumption [54], camera poses are iteratively updated by minimizing the following loss \mathcal{L}_T :

$$\mathcal{L}_T(\xi) = \mathcal{L}_{geo}^{track} + \lambda_p \mathcal{L}_p + \lambda_s \mathcal{L}_s, \quad (23)$$

	ScanNet [5]							Replica [35]								
	0000	0059	0106	0169	0181	0207	Avg.	room_0	room_1	room_2	office_0	office_1	office_2	office_3	office_4	Avg.
NICE-SLAM [54]	8.64	12.25	8.09	10.28	12.93	5.59	9.63	1.69	2.04	1.55	0.99	1.39	3.97	3.08	1.95	2.08
Co-SLAM [42]	7.18	12.29	9.57	6.62	13.43	7.13	9.37	0.65	1.13	1.43	0.55	0.50	0.46	1.40	0.77	0.86
ESLAM [14]	7.3	8.5	7.5	6.5	9.0	5.7	7.42	0.76	0.71	0.56	0.53	0.49	0.58	0.74	0.64	0.62
Point-SLAM [33]	10.24	7.81	8.65	22.16	14.77	9.54	13.97	0.61	0.41	0.37	0.38	0.48	0.54	0.72	0.63	0.52
ADFP [11]	-	10.50	7.48	9.31	-	5.67	8.24	1.39	1.55	2.60	1.09	1.23	1.61	3.61	1.42	1.81
Ours	5.42	5.20	9.11	7.70	10.12	4.91	7.07	0.49	0.46	0.38	0.34	0.35	0.39	0.62	0.60	0.45

Table 1. **Quantitative Tracking Comparison.** We show ATE RMSE \downarrow (cm) results of an average of 3 runs on ScanNet [5] and Replica [35]. We find that our method leads to state-of-the-art performance, improving tracking results on both synthetic and real-world data.

where ξ is the camera poses and λ_p, λ_s are respective loss weighting factors.

4. Experiments

4.1. Experimental Setup

Datasets We evaluate our method on both synthetic and real-world datasets with semantic maps. Following other neural implicit SLAM methods, for the reconstruction quality, we evaluate quantitatively on 8 synthetic scenes from Replica [35] and qualitatively on 6 scenes from ScanNet [5]. As for camera pose accuracy, we evaluate quantitatively on both Replica and ScanNet. The ground-truth poses of Replica are from simulation, while ground-truth poses of ScanNet are obtained with BundleFusion [6].

Metrics We evaluate the reconstruction quality using $DepthL1(cm)$, $Accuracy(cm)$, $Completion(cm)$ and $CompletionRatio(\%)$ with a threshold of 5cm. For evaluation of camera tracking, we adopt $ATE\ RMSE(cm)$ [36]. To evaluate our semantic reconstruction, we report $mIoU$.

Baselines We compare against the state-of-the-art methods NICE-SLAM [54], Co-SLAM [42], ESLAM [14], Point-SLAM [33] and ADFP [11] as our main baselines for reconstruction quality and camera tracking. For semantic evaluation, we compare against the very recent NIDS-SLAM [9] as all other methods do not predict semantic information.

Implementation Details We perform single GPU training (NVIDIA 2080ti), and for experiments with default settings, we use $R_t = 500$ pixels with 30 iterations for tracking and $R = 2000$ pixels for mapping with 100 iterations on Replica, and 200 iterations on ScanNet. For our multi-resolution hash grid settings, we follow Co-SLAM [42]. We use two-layer MLPs with 32 hidden units for each scene representation. We use a learning rate of 0.005 and 0.001 for all learnable parameters on Replica and ScanNet, respectively. For camera poses, we use a learning rate of 0.001 in tracking and 0.0005 in mapping. We use the first layer of ResNet [10] output as our 2D features. Please see the sup. mat. for additional details.

4.2. Tracking Evaluation

We show quantitative results on both Replica [35] and ScanNet [5] in Table 1. Our method demonstrates state-of-the-art



Figure 3. **Qualitative Comparison on ScanNet.** The ground-truth camera trajectory is shown in green and the estimated trajectory is shown in red. Our method predicts more accurate camera trajectories and does not suffer from pose drifting.

tracking performance on the Replica dataset, outperforming other methods over 10% on average in terms of ATE RMSE. It is important to highlight that while both our method and Point-SLAM [33] achieve impressive tracking results on Replica, our method proves to be more robust and effective, particularly in complex real-world scenarios like those encountered in the ScanNet dataset. We attribute this to the fact that Point-SLAM strongly relies on accurate depth supervision, while our approximated occupancy probability formulation provides reliable supervision and our multi-view consistency constraints can effectively address depth map ambiguities even if the depth input is not accurate. Fig. 3 shows a qualitative comparison on ScanNet. Compared with NICE-SLAM [54] and ESLAM [14], our method suffers from less trajectory drifting and, especially for those scenes with more texture, our method can improve ATE RMSE significantly. This highlights the adaptability and robustness of our approach, especially in challenging scenarios, making it a promising solution for practical applications.

4.3. Reconstruction Evaluation

Qualitative and quantitative reconstruction results on Replica [35] are shown in Fig. 4 and Table 2, respectively. We find that SDF-based Co-SLAM [42] leads to good but overly-

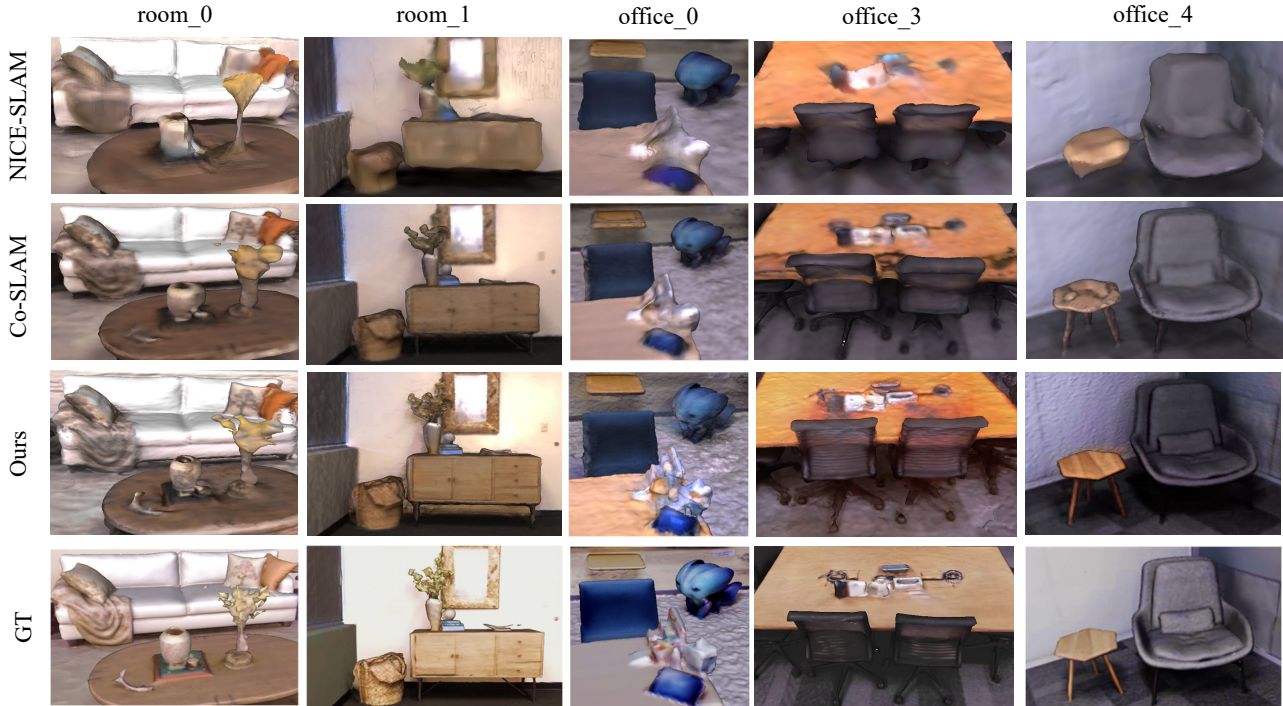


Figure 4. **Qualitative Reconstruction on Replica.** Our method achieves reconstructions with more geometric and appearance details.

	Method	Depth L1↓	Acc.↓	Comp.↓	Comp. Ratio↑
SDF-Based	Co-SLAM	1.58	2.10	2.08	92.99
	ESLAM	1.18	0.97	1.05	98.60
Occupancy-Based	NICE-SLAM	3.53	2.85	3.00	89.33
	ADFP	1.81	2.59	2.28	93.38
	Ours	3.16	2.76	2.74	91.73

Table 2. **Quantitative Reconstruction Comparison on Replica.**

smoothed reconstructions and both Co-SLAM and NICE-SLAM [54] do not lead to satisfactory texture reconstruction. In contrast, our method is able to reconstruct fine geometric structures as well as appearance details (see e.g. the flowers on the table of "room_1" or the side table of "office_4" in Fig. 4). While we improve also quantitatively over NICE-SLAM, we find that the reconstruction metrics favor the overly-smoothed reconstructions from the SDF-based methods such as Co-SLAM, mainly due to the fact that errors in unobserved regions (such as under a table) dominate the evaluation metrics. We plan to investigate appropriate regularization techniques for unobserved regions, e.g. based on diffusion priors, for our image-based approach in the future.

4.4. Semantics Evaluation

Table 3 shows the quantitative evaluation of our method in comparison to another neural semantic SLAM method NIDS-SLAM [9]. We follow NIDS-SLAM and report the mIoU on four scenes. Our method achieves better results despite

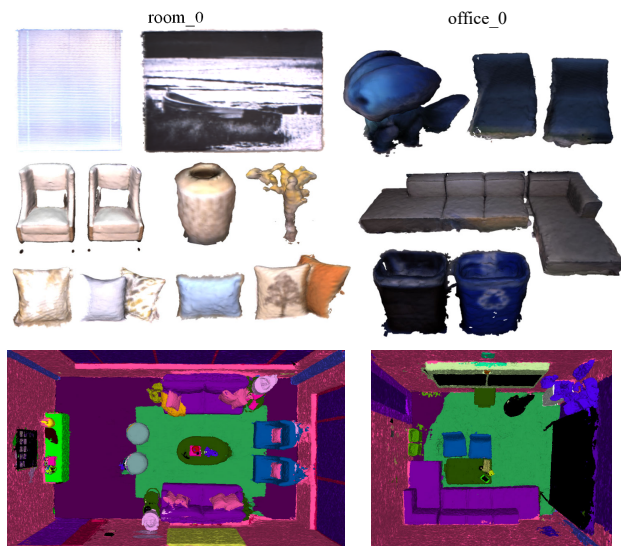


Figure 5. **Decomposed Reconstruction on Replica.** We show the 3D semantic mesh (bottom) and its decomposition with RGB colors (top) of two scenes from Replica.

NIDS-SLAM using ORB-SLAM [25] as its tracking processor, and we are the first neural SLAM method to achieve simultaneous localization, reconstruction and segmentation all at once. Fig. 5 shows class-wise reconstruction results on

Scene	room_0	room_1	room_2	office_0	Avg.
NIDS-SLAM	82.45	84.08	76.99	85.94	82.37
Ours	88.32	84.90	81.20	84.66	84.77

Table 3. **Semantic Segmentation Comparison on Replica.**

Per frame	NICE-SLAM	Co-SLAM	Point-SLAM	Ours
Tracking	1.32 s	0.12 s	0.85 s	0.36 s
Mapping	10.92 s	0.33 s	9.85 s	7.58 s

Table 4. **Runtime Comparison on Replica.**

Method	w/o multi-class	w/o 2D feature	w/o init.	w/o occ. approx.	full model
Replica	1.16	0.71	0.53	0.86	0.49
ScanNet	7.52	6.22	174.4	5.77	5.20

Table 5. **Quantitative Ablation Study (ATE RMSE).**

Replica dataset. Our method can represent and reconstruct each class separately leading to decomposed representations, which can be used as a 3D prior for further downstream tasks.

4.5. Runtime Analysis

We report runtimes on Replica’s room_0 scene in Table 4, using a NVIDIA 2080ti GPU. The tracking and mapping time are reported per frame. We observe that our approach effectively balances performance and runtime considerations, enabling high-fidelity as well as fast SLAM.

4.6. Ablation Study

In Table 5 we report quantitative results for our method where we ablate various components which we discuss in greater detail in the following. We test on scene room_0 from Replica and scene 0059 from ScanNet.

New Class Initialization. We find that if a new class representation is not initialized appropriately before it is added to the system, it leads to inadequate RGB predictions not only for the new class but also for existing classes due to a bleeding effect. It is important to note that this in turn also leads to an increased camera pose error and sometimes causing further tracking failures. This is in particular visible on the real-world dataset ScanNet.

Multi-Class Scene Representations. We ablate our multi-class scene representations by using only a single representation during the whole process. Table 5 shows that our full mode leads to higher accuracy considering ATE RMSE than only using a single geometry representation. The difference is larger on ScanNet where the input data is noisy and the size of the scene is larger compared to Replica.

Conditional Image Feature Input. Image features serve as a conditional input for our system, enforcing a multi-view geometry constraint and enhancing the texture prediction. Table 5 shows a decline in ATE RMSE on both synthetic and

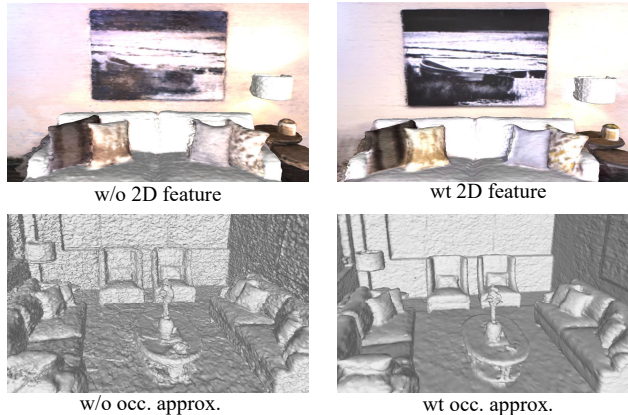


Figure 6. **Ablation Study.** We show that 2D image feature can provide conditional information for reconstruction (top). And occupancy probability approximation can help to smooth the reconstruction (bottom).

real-world datasets when removing the conditional input. Fig. 6 shows a visual comparison of the reconstructed meshes. We find that without 2D image features, the reconstruction become smoother and contain less details.

Occupancy Probability Approximation. Finally, We investigate the effectiveness of our occupancy probability approximation and show a qualitative comparison in Fig. 6. The output mesh tends to be noisier and artifacts appear. In contrast, the meshes of our full model are smoother while containing fine details. Table 5 further shows that our full model also leads to better tracking performance.

5. Conclusion

We present DNS SLAM, the first method that uses a neural representation for simultaneously localization, reconstruction and segmentation. We propose to use a semantically decomposed scene representation in combination with conditional 2D image features, enforcing stronger geometric constraints and hence enabling better tracking and more detailed appearance prediction while being more robust to noisy depth inputs. Our occupancy probability approximation serves as a strong supervision signal, enabling accurate and smooth mesh reconstruction. Extensive experiments show that our method significantly improves the tracking accuracy compared to state-of-the-art baselines while also providing class-wise decompositions.

Limitations. Our method relies on RGB-D and semantic maps as input. While being more robust to noisy depth inputs than previous works, we plan to investigate RGB only input in the future.

References

- [1] Dejan Azinović, Ricardo Martin-Brualla, Dan B Goldman, Matthias Nießner, and Justus Thies. Neural rgb-d surface reconstruction. In *Proceedings of the IEEE/CVF Conference on Computer Vision and Pattern Recognition*, pages 6290–6301, 2022. [2](#)
- [2] Wenjing Bian, Zirui Wang, Kejie Li, Jia-Wang Bian, and Victor Adrian Prisacariu. Nope-nerf: Optimising neural radiance field with no pose prior. In *Proceedings of the IEEE/CVF Conference on Computer Vision and Pattern Recognition*, pages 4160–4169, 2023. [2](#)
- [3] Michael Bloesch, Jan Czarnowski, Ronald Clark, Stefan Leutenegger, and Andrew J Davison. Codeslam—learning a compact, optimisable representation for dense visual slam. In *Proceedings of the IEEE conference on computer vision and pattern recognition*, pages 2560–2568, 2018. [2](#)
- [4] Zhiqin Chen and Hao Zhang. Learning implicit fields for generative shape modeling. In *CVPR*, 2019. [2](#)
- [5] Angela Dai, Angel X. Chang, Manolis Savva, Maciej Halber, Thomas Funkhouser, and Matthias Nießner. Scannet: Richly-annotated 3d reconstructions of indoor scenes. In *CVPR*, 2017. [6](#), [12](#)
- [6] Angela Dai, Matthias Nießner, Michael Zollhöfer, Shahram Izadi, and Christian Theobalt. Bundlefusion: Real-time globally consistent 3d reconstruction using on-the-fly surface reintegration. *ACM Transactions on Graphics (ToG)*, 36(4):1, 2017. [2](#), [6](#)
- [7] Andrew J Davison, Ian D Reid, Nicholas D Molton, and Olivier Stasse. Monoslam: Real-time single camera slam. *IEEE TPAMI*, 29(6):1052–1067, 2007. [1](#), [2](#)
- [8] Haoyu Guo, Sida Peng, Haotong Lin, Qianqian Wang, Guofeng Zhang, Hujun Bao, and Xiaowei Zhou. Neural 3d scene reconstruction with the manhattan-world assumption. In *Proceedings of the IEEE/CVF Conference on Computer Vision and Pattern Recognition*, pages 5511–5520, 2022. [2](#)
- [9] Yasaman Haghighi, Suryansh Kumar, Jean Philippe Thiran, and Luc Van Gool. Neural implicit dense semantic slam. *arXiv preprint arXiv:2304.14560*, 2023. [6](#), [7](#)
- [10] Kaiming He, Xiangyu Zhang, Shaoqing Ren, and Jian Sun. Deep residual learning for image recognition. In *CVPR*, pages 770–778, 2016. [4](#), [6](#), [12](#)
- [11] Pengchong Hu and Zhizhong Han. Learning neural implicit through volume rendering with attentive depth fusion priors. In *Advances in Neural Information Processing Systems (NeurIPS)*, 2023. [1](#), [2](#), [6](#)
- [12] Jiahui Huang, Shi-Sheng Huang, Haoxuan Song, and Shi-Min Hu. Di-fusion: Online implicit 3d reconstruction with deep priors. In *Proceedings of the IEEE/CVF Conference on Computer Vision and Pattern Recognition*, pages 8932–8941, 2021. [1](#)
- [13] Shahram Izadi, David Kim, Otmar Hilliges, David Molyneaux, Richard Newcombe, Pushmeet Kohli, Jamie Shotton, Steve Hodges, Dustin Freeman, Andrew Davison, et al. Kinectfusion: real-time 3d reconstruction and interaction using a moving depth camera. In *Proceedings of the 24th annual ACM symposium on User interface software and technology*, pages 559–568, 2011. [1](#), [2](#)
- [14] Mohammad Mahdi Johari, Camilla Carta, and François Fleuret. Eslam: Efficient dense slam system based on hybrid representation of signed distance fields. In *Proceedings of the IEEE/CVF Conference on Computer Vision and Pattern Recognition*, pages 17408–17419, 2023. [1](#), [2](#), [6](#), [12](#)
- [15] Olaf Kähler, Victor Prisacariu, Julien Valentin, and David Murray. Hierarchical voxel block hashing for efficient integration of depth images. *IEEE Robotics and Automation Letters*, 1(1):192–197, 2015. [2](#)
- [16] Georg Klein and David Murray. Parallel tracking and mapping for small ar workspaces. In *2007 6th IEEE and ACM international symposium on mixed and augmented reality*, pages 225–234. IEEE, 2007. [1](#), [2](#)
- [17] Xin Kong, Shikun Liu, Marwan Taher, and Andrew J Davison. vmap: Vectorised object mapping for neural field slam. In *Proceedings of the IEEE/CVF Conference on Computer Vision and Pattern Recognition*, pages 952–961, 2023. [1](#), [4](#)
- [18] Abhijit Kundu, Kyle Genova, Xiaoqi Yin, Alireza Fathi, Caroline Pantofaru, Leonidas J Guibas, Andrea Tagliasacchi, Frank Dellaert, and Thomas Funkhouser. Panoptic neural fields: A semantic object-aware neural scene representation. In *Proceedings of the IEEE/CVF Conference on Computer Vision and Pattern Recognition*, pages 12871–12881, 2022. [4](#)
- [19] Jonathan Long, Evan Shelhamer, and Trevor Darrell. Fully convolutional networks for semantic segmentation. In *Proceedings of the IEEE conference on computer vision and pattern recognition*, pages 3431–3440, 2015. [4](#)
- [20] Lars M. Mescheder, Michael Oechsle, Michael Niemeyer, Sebastian Nowozin, and Andreas Geiger. Occupancy networks: Learning 3d reconstruction in function space. In *CVPR*, 2019. [2](#)
- [21] Ben Mildenhall, Pratul P Srinivasan, Matthew Tancik, Jonathan T Barron, Ravi Ramamoorthi, and Ren Ng. Nerf: Representing scenes as neural radiance fields for view synthesis. *Communications of the ACM*, 65(1):99–106, 2021. [2](#), [4](#)
- [22] Ben Mildenhall, Peter Hedman, Ricardo Martin-Brualla, Pratul P Srinivasan, and Jonathan T Barron. Nerf in the dark: High dynamic range view synthesis from noisy raw images. In *Proceedings of the IEEE/CVF Conference on Computer Vision and Pattern Recognition*, pages 16190–16199, 2022. [2](#)
- [23] Thomas Müller, Brian McWilliams, Fabrice Rousselle, Markus Gross, and Jan Novák. Neural importance sampling. *ACM Transactions on Graphics (ToG)*, 38(5):1–19, 2019. [3](#)
- [24] Thomas Müller, Alex Evans, Christoph Schied, and Alexander Keller. Instant neural graphics primitives with a multiresolution hash encoding. *ACM Transactions on Graphics (ToG)*, 41(4):1–15, 2022. [2](#), [3](#)
- [25] Raul Mur-Artal, Jose Maria Martinez Montiel, and Juan D Tardos. Orb-slam: a versatile and accurate monocular slam system. *IEEE transactions on robotics*, 31(5):1147–1163, 2015. [1](#), [2](#), [4](#), [7](#)
- [26] Richard A Newcombe, Steven J Lovegrove, and Andrew J Davison. Dtam: Dense tracking and mapping in real-time. In *2011 international conference on computer vision*, pages 2320–2327. IEEE, 2011. [2](#)
- [27] Michael Niemeyer, Lars M. Mescheder, Michael Oechsle, and Andreas Geiger. Differentiable volumetric rendering:

- Learning implicit 3d representations without 3d supervision. In *CVPR*, 2020. 5
- [28] Matthias Nießner, Michael Zollhöfer, Shahram Izadi, and Marc Stamminger. Real-time 3d reconstruction at scale using voxel hashing. *ACM Transactions on Graphics (ToG)*, 32(6): 1–11, 2013. 2
- [29] Michael Oechsle, Songyou Peng, and Andreas Geiger. Unisurf: Unifying neural implicit surfaces and radiance fields for multi-view reconstruction. In *Proceedings of the IEEE/CVF International Conference on Computer Vision*, pages 5589–5599, 2021. 4
- [30] Jeong Joon Park, Peter R. Florence, Julian Straub, Richard A. Newcombe, and Steven Lovegrove. DeepSDF: Learning continuous signed distance functions for shape representation. In *CVPR*, 2019. 2
- [31] Christian Reiser, Songyou Peng, Yiyi Liao, and Andreas Geiger. Kilonerf: Speeding up neural radiance fields with thousands of tiny mlps. In *ICCV*, 2021. 4
- [32] Olaf Ronneberger, Philipp Fischer, and Thomas Brox. U-net: Convolutional networks for biomedical image segmentation. In *Medical Image Computing and Computer-Assisted Intervention–MICCAI 2015: 18th International Conference, Munich, Germany, October 5–9, 2015, Proceedings, Part III 18*, pages 234–241. Springer, 2015. 4
- [33] Erik Sandström, Yue Li, Luc Van Gool, and Martin R Oswald. Point-slam: Dense neural point cloud-based slam. In *Proceedings of the IEEE/CVF International Conference on Computer Vision*, pages 18433–18444, 2023. 1, 2, 6, 12
- [34] Thomas Schops, Torsten Sattler, and Marc Pollefeys. Bad slam: Bundle adjusted direct rgb-d slam. In *Proceedings of the IEEE/CVF Conference on Computer Vision and Pattern Recognition*, pages 134–144, 2019. 2
- [35] Julian Straub, Thomas Whelan, Lingni Ma, Yufan Chen, Erik Wijmans, Simon Green, Jakob J Engel, Raul Mur-Artal, Carl Ren, Shobhit Verma, et al. The replica dataset: A digital replica of indoor spaces. *arXiv preprint arXiv:1906.05797*, 2019. 6, 12
- [36] Jürgen Sturm, Nikolas Engelhard, Felix Endres, Wolfram Burgard, and Daniel Cremers. A benchmark for the evaluation of rgb-d slam systems. In *2012 IEEE/RSJ international conference on intelligent robots and systems*, pages 573–580. IEEE, 2012. 6
- [37] Edgar Sucar, Kentaro Wada, and Andrew Davison. Nodeslam: Neural object descriptors for multi-view shape reconstruction. In *2020 International Conference on 3D Vision (3DV)*, pages 949–958. IEEE, 2020. 2
- [38] Edgar Sucar, Shikun Liu, Joseph Ortiz, and Andrew J Davison. imap: Implicit mapping and positioning in real-time. In *Proceedings of the IEEE/CVF International Conference on Computer Vision*, pages 6229–6238, 2021. 1, 2
- [39] Zachary Teed and Jia Deng. DeepV2d: Video to depth with differentiable structure from motion. *arXiv preprint arXiv:1812.04605*, 2018. 2
- [40] Zachary Teed and Jia Deng. Droid-slam: Deep visual slam for monocular, stereo, and rgb-d cameras. *NeurIPS*, 34:16558–16569, 2021. 1, 2
- [41] Emanuele Vespa, Nikolay Nikolov, Marius Grimm, Luigi Nardi, Paul HJ Kelly, and Stefan Leutenegger. Efficient octree-based volumetric slam supporting signed-distance and occupancy mapping. *IEEE Robotics and Automation Letters*, 3(2):1144–1151, 2018. 2
- [42] Hengyi Wang, Jingwen Wang, and Lourdes Agapito. Co-slam: Joint coordinate and sparse parametric encodings for neural real-time slam. In *Proceedings of the IEEE/CVF Conference on Computer Vision and Pattern Recognition*, pages 13293–13302, 2023. 1, 2, 3, 5, 6, 12
- [43] Silvan Weder, Johannes Schonberger, Marc Pollefeys, and Martin R Oswald. Routedfusion: Learning real-time depth map fusion. In *Proceedings of the IEEE/CVF Conference on Computer Vision and Pattern Recognition*, pages 4887–4897, 2020. 2
- [44] Silvan Weder, Johannes L Schonberger, Marc Pollefeys, and Martin R Oswald. Neuralfusion: Online depth fusion in latent space. In *Proceedings of the IEEE/CVF Conference on Computer Vision and Pattern Recognition*, pages 3162–3172, 2021. 1, 2
- [45] Thomas Whelan, Stefan Leutenegger, Renato Salas-Moreno, Ben Glocker, and Andrew Davison. Elasticfusion: Dense slam without a pose graph. *Robotics: Science and Systems*, 2015. 2
- [46] Nan Yang, Lukas von Stumberg, Rui Wang, and Daniel Cremers. D3vo: Deep depth, deep pose and deep uncertainty for monocular visual odometry. In *Proceedings of the IEEE/CVF conference on computer vision and pattern recognition*, pages 1281–1292, 2020. 2
- [47] Alex Yu, Vickie Ye, Matthew Tancik, and Angjoo Kanazawa. pixelnerf: Neural radiance fields from one or few images. In *Proceedings of the IEEE/CVF Conference on Computer Vision and Pattern Recognition*, pages 4578–4587, 2021. 2, 4
- [48] Zehao Yu, Songyou Peng, Michael Niemeyer, Torsten Sattler, and Andreas Geiger. Monosdf: Exploring monocular geometric cues for neural implicit surface reconstruction. *Advances in neural information processing systems*, 35:25018–25032, 2022. 2
- [49] Richard Zhang, Phillip Isola, Alexei A Efros, Eli Shechtman, and Oliver Wang. The unreasonable effectiveness of deep features as a perceptual metric. In *Proceedings of the IEEE conference on computer vision and pattern recognition*, pages 586–595, 2018. 12
- [50] Shuaifeng Zhi, Michael Bloesch, Stefan Leutenegger, and Andrew J Davison. Scenecode: Monocular dense semantic reconstruction using learned encoded scene representations. In *Proceedings of the IEEE/CVF Conference on Computer Vision and Pattern Recognition*, pages 11776–11785, 2019. 2
- [51] Shuaifeng Zhi, Tristan Laidlow, Stefan Leutenegger, and Andrew J Davison. In-place scene labelling and understanding with implicit scene representation. In *Proceedings of the IEEE/CVF International Conference on Computer Vision*, pages 15838–15847, 2021. 2
- [52] Huizhong Zhou, Benjamin Ummenhofer, and Thomas Brox. Deeptam: Deep tracking and mapping. In *Proceedings of the European conference on computer vision (ECCV)*, pages 822–838, 2018. 2
- [53] Xingyi Zhou, Rohit Girdhar, Armand Joulin, Philipp Krähenbühl, and Ishan Misra. Detecting twenty-thousand

classes using image-level supervision. In *European Conference on Computer Vision*, pages 350–368. Springer, 2022. 4

- [54] Zihan Zhu, Songyou Peng, Viktor Larsson, Weiwei Xu, Hujun Bao, Zhaopeng Cui, Martin R Oswald, and Marc Pollefeys. Nice-slam: Neural implicit scalable encoding for slam. In *Proceedings of the IEEE/CVF Conference on Computer Vision and Pattern Recognition*, pages 12786–12796, 2022. 1, 2, 5, 6, 7, 12

A. Implementation details

A.1. Hyperparameters

In the following, we report implementation details and hyperparameters used for our method to achieve high-accuracy tracking and mapping.

Default Settings. We use $L = 16$ level hash grids with $R_{min} = 16$ to R_{max} , where we set the maximal voxel size to 2cm for determining R_{max} . We use 16 bins for the OneBlob encoding of each dimension. For the network heads, we use two-layer MLPs with 32 hidden units for each scene presentation. The loss weights we set to $\lambda_p = 3$, $\lambda_s = 0.1$, $\lambda_l = 10$, $\lambda_o = 10$, $\lambda_{fs} = 5$ and the truncation distance tr is set to 10cm. For ray sampling, we use $M_s = 15$ and $M_a = 32$ points. In a forward pass, We sample $R_t = 500$ pixels during tracking and $R = 2000$ pixels during mapping. In tracking, we estimate camera pose for each frame. In mapping, bundle adjustment will be applied every 5 frame, which updates the scene representations and camera poses jointly. The window size W for bundle adjustment is set to 5 keyframes. For initialization, we start with 500 iterations for the first frame.

Replica. For the Replica dataset [35], we perform 30 iterations for tracking and 100 iterations for mapping. We choose a keyframe every 30 frames. We set the learning rate for all learnable parameters to 0.005 except for the camera parameters for which we use a learning rate of 0.001 in tracking and 0.0005 in mapping.

ScanNet. For the ScanNet dataset [5], we use $L = 20$ level hash grids with $R_{min} = 16$ to R_{max} , where we use a maximal voxel size of 4cm to determine R_{max} . We perform 30 iterations of tracking and 200 iterations of mapping iteratively. We choose a keyframe every 15 frames. We set the learning rate for all learnable parameters to 0.001 except for the camera parameters for which we use a learning rate of 0.001 during tracking and 0.0005 during mapping.

B. Additional Experimental Results

B.1. More Reconstruction Results

In this section, we report additional reconstruction results. Fig. 8 shows a top-down view comparison and Fig. 9 shows zoom-in views on Replica. Even though SDF-based methods such as Co-SLAM [42] and ESLAM [14] lead to better results in terms of quantitative metrics, we observe that our method leads to meshes with more geometric details. For example, our method reconstructs the individual objects in the scene (see e.g. the tiny object on the table of "room_0" in Fig. 9) while the other methods struggle to do so. We also show reconstruction results on ScanNet. Fig. 10 shows that our method leads to better reconstructions while NICE-SLAM [54] and ESLAM [14] show limited reconstruction capabilities on these challenging real-world scenes (see e.g.

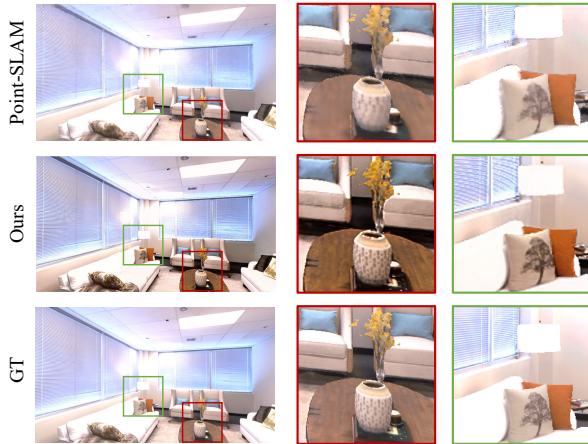


Figure 7. **Rendering Results on Replica.**

the water dispenser of "0059" and the toilet of "0207" in Fig. 10).

B.2. More Semantic Results on Synthetic Scenes

We first show qualitative results for semantic segmentation compared with the ground-truth in Fig. 11. We are able to accurately segment the 3D space with errors only occur near the boundaries of objects. Fig. 12 shows decomposition results of the remaining scenes. Our method enables class-wise decomposed reconstructions with fine geometric details.

B.3. Novel-View Synthesis Evaluation

Table 6 shows a comparison for novel view synthesis performance across 8 scenes from Replica. We follow the evaluation protocol in [33]. Note that our method can reach on par results with Point-SLAM on SSIM and LPIPs [49] without generating intermediate point cloud representations which requires significant computational resource and time. Further, Fig. 7 shows that our method better maintains the image structure of the ground truth next to the color, which is especially important for real-world scenes where the input color images can suffer from bad light conditions or motion blur. We hypothesize that this is largely coming from incorporating a pre-trained ResNet [10] model, which was trained for image recognition, and in turn tends to preserve texture details of images instead of only the RGB color. We plan to implement an additional exposure compensation mechanism to further improve color prediction in future research.

B.4. Limitation Discussion

Fig. 13 shows our reconstruction of an unobserved region. We observe that our occupancy-based approach tends to predict a surface continuation in the unobserved region, while being freespace in the ground truth. We plan to investigate more complex regularization strategies and partial infilling

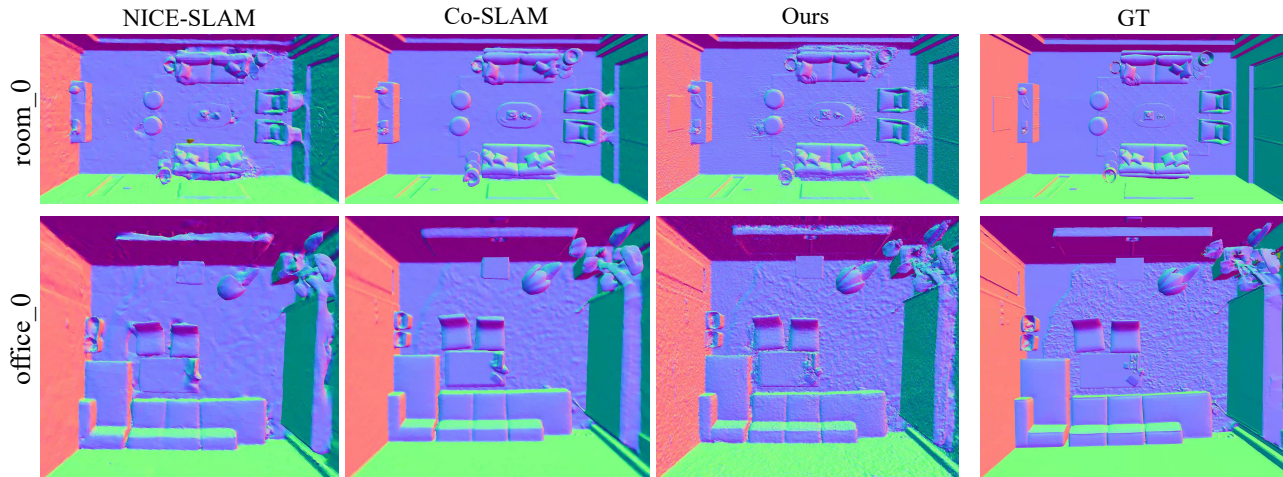


Figure 8. Normal Map of Reconstructions on Replica.

Method	PSNR(dB) \uparrow	SSIM \uparrow	LPIPS \downarrow
NICE-SLAM	24.42	0.809	0.233
Point-SLAM	35.17	0.975	0.124
<i>Ours</i>	22.96	0.963	0.119

Table 6. Rendering Results of an average of 3 runs on Replica.

approaches to make our approach more robust for sparser captures.

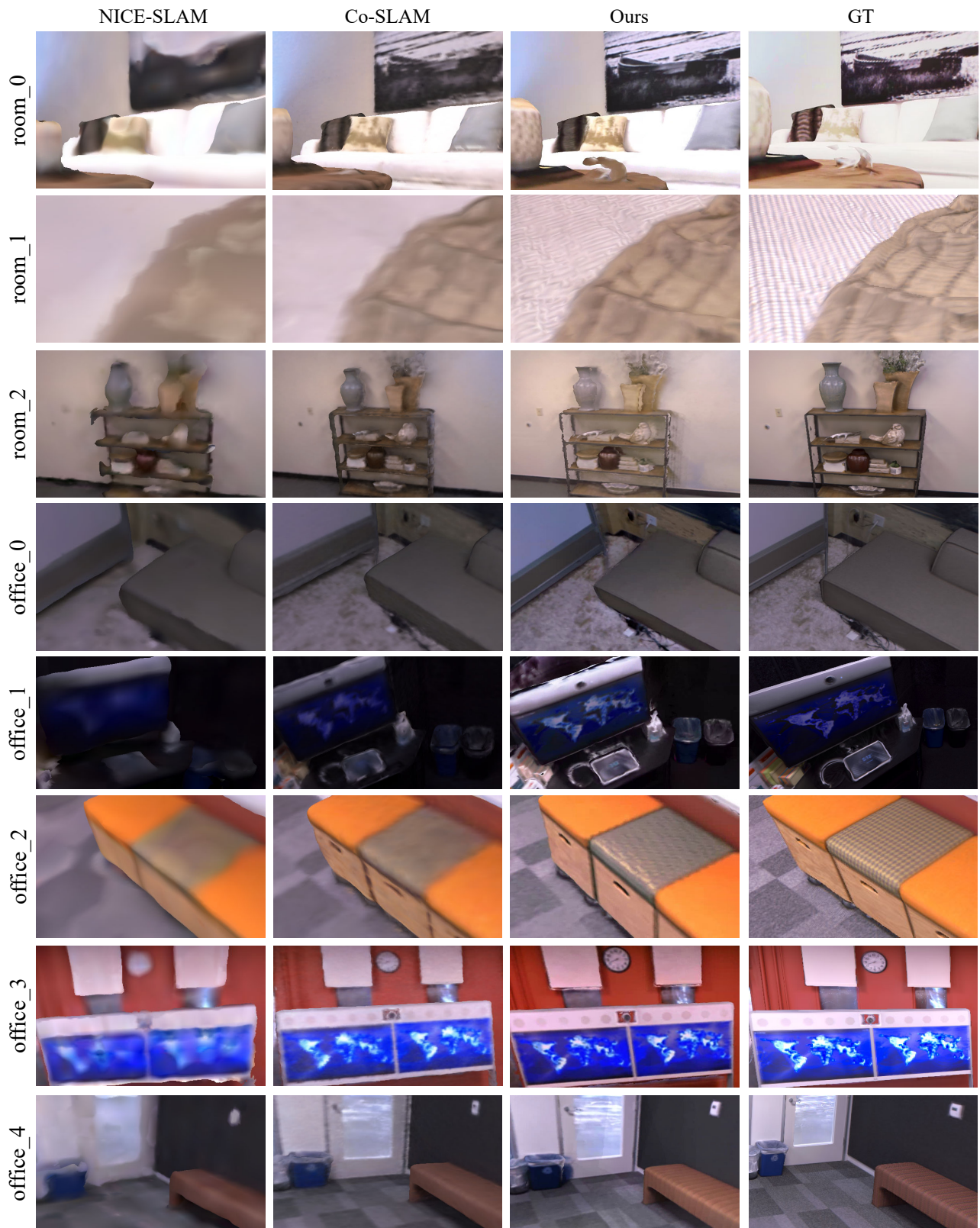


Figure 9. Zoom-In View of Reconstructions on Replica.

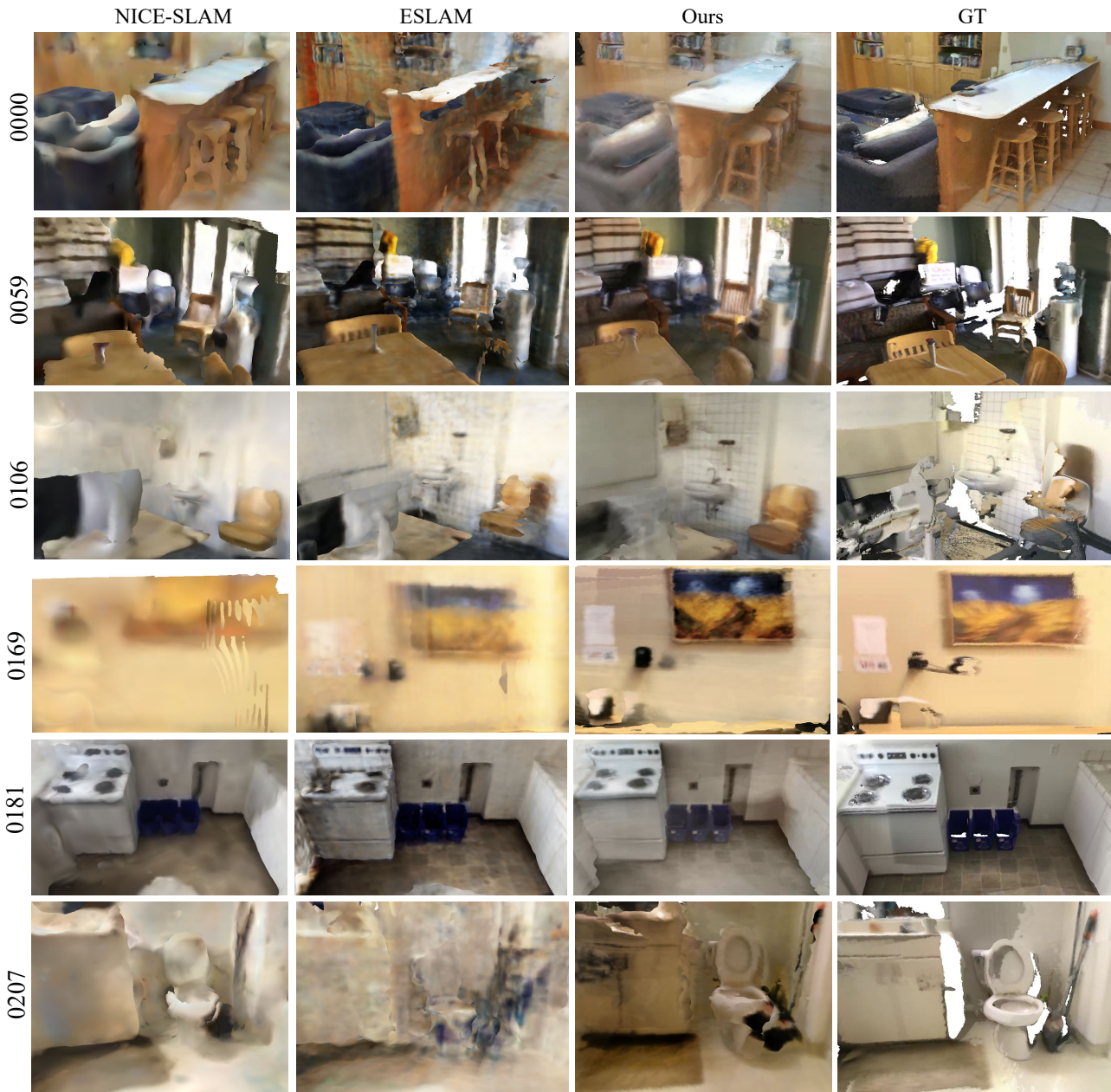


Figure 10. Zoom-In View of Reconstructions on ScanNet.

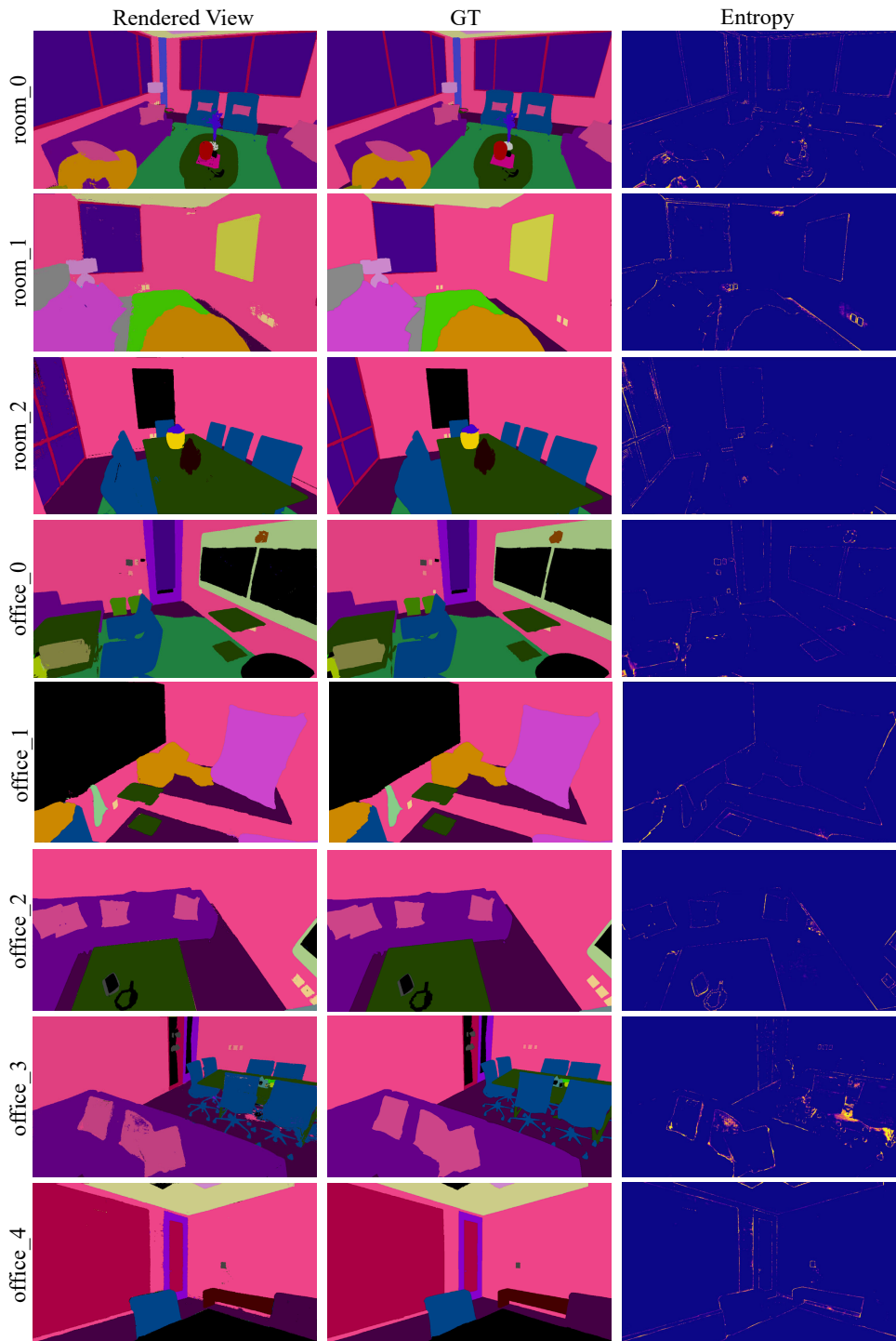


Figure 11. **Semantic Segmentation on Replica.** From left to right: rendered semantic labels, ground-truth semantic labels and information entropy, highlighting regions with noisy predictions.

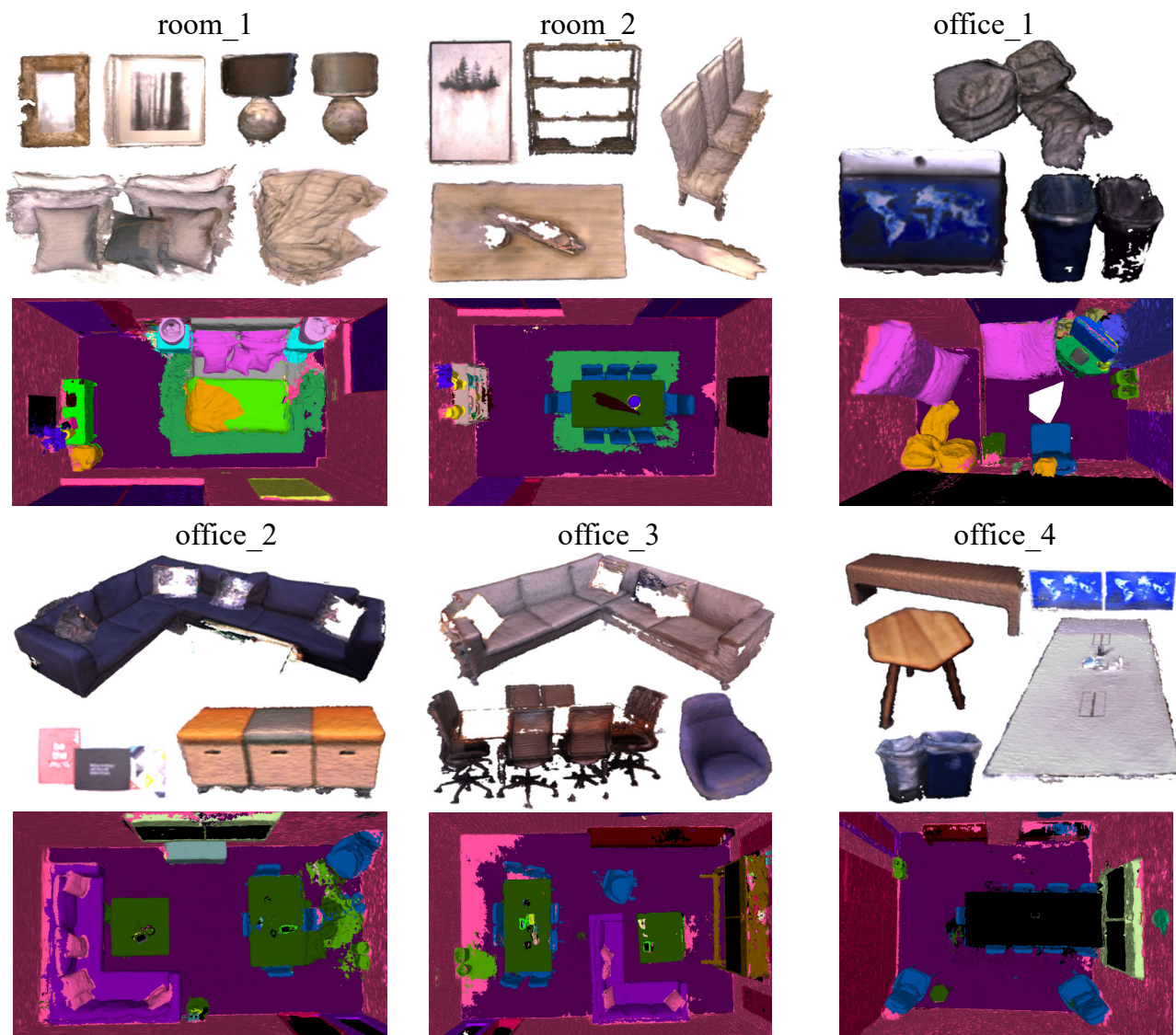


Figure 12. Decomposed Reconstruction on Replica

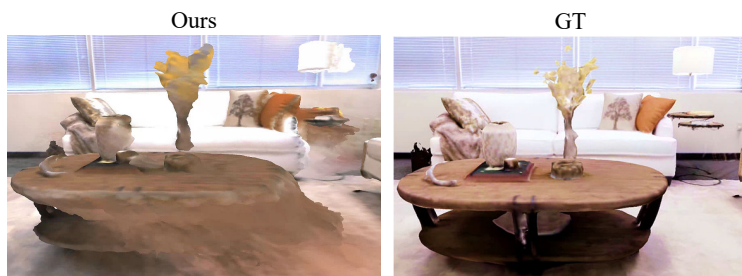


Figure 13. Failure Case on Replica. .